Biophysical *Journal*
Article

Biophysical Society

Detailed Analyses of Stall Force Generation in *Mycoplasma mobile* Gliding

Masaki Mizutani,[1] Isil Tulum,[1,2] Yoshiaki Kinosita,[3] Takayuki Nishizaka,[3] and Makoto Miyata[1,2,*]
[1]Department of Biology, Graduate School of Science, Osaka City University, Sumiyoshi-ku, Osaka, Japan; [2]The OCU Advanced Research Institute for Natural Science and Technology, Osaka City University, Sumiyoshi-ku, Osaka, Japan; and [3]Department of Physics, Faculty of Science, Gakushuin University, Toshima-ku, Tokyo, Japan

ABSTRACT *Mycoplasma mobile* is a bacterium that uses a unique mechanism to glide on solid surfaces at a velocity of up to 4.5 μm/s. Its gliding machinery comprises hundreds of units that generate the force for gliding based on the energy derived from ATP; the units catch and pull sialylated oligosaccharides fixed to solid surfaces. In this study, we measured the stall force of wild-type and mutant strains of *M. mobile* carrying a bead manipulated using optical tweezers. The strains that had been enhanced for binding exhibited weaker stall forces than the wild-type strain, indicating that stall force is related to force generation rather than to binding. The stall force of the wild-type strain decreased linearly from 113 to 19 picoNewtons after the addition of 0–0.5 mM free sialyllactose (a sialylated oligosaccharide), with a decrease in the number of working units. After the addition of 0.5 mM sialyllactose, the cells carrying a bead loaded using optical tweezers exhibited stepwise movements with force increments. The force increments ranged from 1 to 2 picoNewtons. Considering the 70-nm step size, this small-unit force may be explained by the large gear ratio involved in the *M. mobile* gliding machinery.

INTRODUCTION

Members of the bacterial class *Mollicutes*, which includes the genus *Mycoplasma*, are parasitic and occasionally commensal bacteria that are characterized by small cells and genomes and by the absence of a peptidoglycan layer (1,2). Dozens of parasitic *Mycoplasma* species, such as the fish pathogen *Mycoplasma mobile* (3–5) and the human pathogen *Mycoplasma pneumoniae* (6–8), have protrusions and exhibit gliding motility in the direction of the protrusions on solid surfaces, which enables mycoplasmas to parasitize other organisms. Interestingly, *Mycoplasma* gliding does not involve flagella or pili and is completely unrelated to other bacterial motility systems or the conventional motor proteins that are common in eukaryotic motility.

M. mobile, which can be isolated from the gills of freshwater fish, is a fast-gliding *Mycoplasma* (9–13). It glides smoothly and continuously on glass at an average speed of 2.0–4.5 μm/s, or 3–7 times the length of the cell per second. A working model called the centipede or power stroke model has been proposed to explain the gliding mechanism of *M. mobile*: the cells repeatedly catch, pull, drag, and release the sialylated oligosaccharides (SOs) on solid surfaces (3–5,14). The gliding machinery comprises internal and surface structures (15–19). The internal structure includes the α- and β-subunit paralogs of F-type ATPase/synthase and generates the force for gliding based on the energy derived from ATP (18–22). The force is probably transmitted across the cell membrane to the surface structure, which is composed of at least three huge proteins: Gli123, Gli521, and Gli349 (15–17,23). Gli521, the crank protein, transmits the interior force of the cell to Gli349, with actual structural changes (17,24). Gli349, the leg protein, extends after thermal fluctuation and catches the SOs, which are the predominant structures on animal cell surfaces (Fig. 1 *A*) (9,25–28). The cells always glide in the direction of the machinery, which may be a result of the directed binding of the cells on solid surfaces (3,29). In theory, hundreds of gliding units on the cell surface should act cooperatively to enable smooth gliding (Fig. 1 *B*) (15,27,30). To examine this working model in detail, it is necessary to investigate the behavior of the individual units. Recently, the discrete movements involved in gliding motility, which are possibly attributable to single-leg movements, have been observed by controlling the working leg number after the addition of free SOs (22,27). In this study, we focused on the pulling force exerted on the solid surface because the generation of force has not been properly investigated, with the

Submitted August 14, 2017, and accepted for publication January 29, 2018.

*Correspondence: miyata@sci.osaka-cu.ac.jp

Yoshiaki Kinosita's present address is Institute for Biology II, Freiburg University, Freiburg, Germany

Editor: Kinneret Keren.

https://doi.org/10.1016/j.bpj.2018.01.029

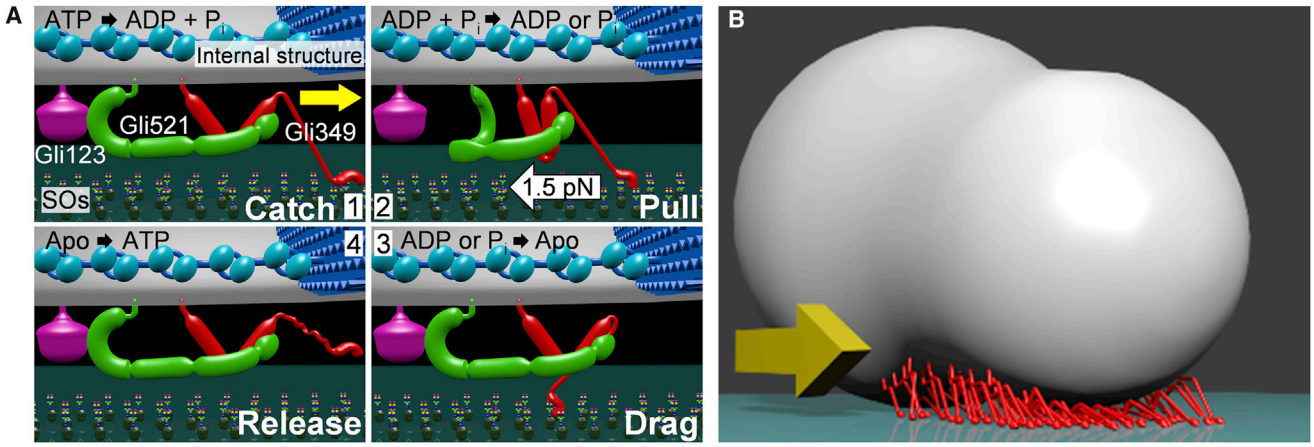

FIGURE 1 Schematic illustration of gliding mechanism. (*A*) Shown is a working model for the gliding mechanism (based on previous experiments) focusing on the single unit of machinery. The unit consists of an internal structure (*upper blue*) and three huge proteins: Gli123 (*purple*), Gli349 (*red*), and Gli521 (*green*) on the cell surface. The mechanism is divided into stages (1) through (4). The illustration is approximately in scale, as shown by Gli521 (120 nm) and Gli349 (95 nm). The gliding direction is shown by a yellow arrow. The leg composed of Gli349 catches an SO on the solid surface tightly after thermal fluctuation (1). The leg pulls the SO, resulting in the cell propulsion. The unit force was estimated around 1.5 pN in this study (see Fig. 6) (2). Continuous displacement of the cell caused by other legs pulls the leg after stroke, resulting in drag generation (3). The leg is detached from the SO by the continuous displacement (4). (*B*) About 75 legs (*red*) sticking out from the cell can work simultaneously. The cell glides in the direction of the yellow arrow. Unbound legs are not illustrated. APO, apoenzyme; P_i, phosphate. To see this figure in color, go online.

exception of the force-velocity relationship of the wild-type (WT) strain under limited conditions (11). Therefore, in this study, we quantitatively measured the pulling forces of several strains of whole cells under various conditions using optical tweezers (11,29,31–33) and characterized the force generated by the gliding machinery.

MATERIALS AND METHODS

Strains and cultivation

The *M. mobile* strain 163K (American Type Culture Collection 43663) was used as the WT strain, and its nine mutants were grown in Aluotto medium at 25°C, as previously described (12,28,34,35).

Surface modifications of *M. mobile* cells and polystyrene beads

The cultured cells were washed with phosphate-buffered saline with glucose (PBS/G) consisting of 75 mM sodium phosphate (pH 7.3), 68 mM NaCl, and 20 mM glucose; suspended in 1.0 mM Sulfo-NHS-LC-LC-Biotin (Thermo Fisher Scientific, Waltham, MA) in PBS/G; and kept for 15 min at room temperature (RT), as previously described (28–30,33,36,37). Polystyrene beads (1.0 μm in diameter) (Polysciences, Warrington, PA) were coated with avidin (Sigma-Aldrich, St. Louis, MO), as previously described (29).

Force measurements

The avidin-coated beads were attached to biotinylated cells in two different ways according to the concentrations of free sialyllactose (SL) used in the experiments. In force measurements under 0–0.13 mM SL conditions, the biotinylated cells were inserted into a tunnel chamber that had been pre-coated with 10% horse serum (20,27,30). Avidin-coated beads were sonicated, inserted into the tunnel chamber with various concentrations of free SL in PBS/G, and bound to the cells (33). In force measurements under 0.25–0.50 mM SL conditions, avidin-coated beads were sonicated and mixed with biotinylated cells in a microtube and kept for 10–30 min at RT. Then, the mixture was inserted into a tunnel chamber and kept for 15 min at RT. The chamber was washed with PBS/G and the PBS/G was replaced by various concentrations of free SL in PBS/G. Both ends of the tunnel were sealed with nail polish. The bead movements were recorded at 200 or 500 frames per second and analyzed by displacement of up to 200 nm from the trap center (the linear range of the laser trap) using ImageJ 1.43u (http://rsb.info.nih.gov/ij/) and IGOR Pro 6.33J (WaveMetrics, Portland, OR) software packages (22,29,33,38).

Genome sequencing of the various strains

All the strains were plated and isolated as previously described (19). The genomic DNA of each strain was isolated using a QIAGEN DNeasy Blood & Tissue kit (QIAGEN, Hilden, Germany). The isolated genomic DNA was sequenced using MiSeq (Illumina, San Diego, CA) and mapped by CLC Genomics Workbench 8 (QIAGEN).

Characterization of binding and gliding of the various strains

All the strains were cultured to reach an optical density of 0.08 at 600 nm. They were then suspended and inserted into a tunnel chamber. Cell behavior was recorded and analyzed as previously reported (27,30,35).

RESULTS

Stall force measurement

The propelling force in *M. mobile* cells has been measured using optical tweezers (11). A bead bound to a cell was trapped by a highly focused laser beam, and the force was calculated by measuring the distance between the center of the bead and the trap; the force acting on the bead increased

linearly with the displacement from the trap center (11,29,33). In the present study, *M. mobile* cells, which had been biotinylated and suspended in PBS/G, were inserted into a tunnel chamber. Polystyrene beads coated with avidin (1.0 μm in diameter) were subsequently added to the tunnel. A bead trapped using optical tweezers was attached to the back end of the gliding cell by exploiting the avidin-biotin interaction (29,36,37). The cell pulled the bead from the trap center (Fig. 2 *A*; see also Movie S1). Starting from 0 s, the pulling force increased and reached a plateau at ~40 s. The maximal value of the average of 25 data points was used as the stall force (Fig. 2 *B*). The stall force of the WT strain was 113 ± 32 picoNewtons (pN) ($n = 50$).

To determine the proteins involved in force generation or force transmission, we measured the stall force in the WT strain of *M. mobile* to compare it with that in six previously isolated strains with known gliding speeds and/or binding activities (12,21,35). The *gli521* (P476R) mutant of protein Gli521 has a single-amino-acid substitution (proline for arginine at the 476th position) (21), but mutations in other strains have not been described. The pulling forces of the mutants increased from 0 s and stalled at 20–50 s. The stall force of the m14 strain—110 ± 29 pN ($n = 29$)—was not significantly different from that of the WT strain ($p = 0.1 > 0.05$, according to Student's *t*-test). The stall forces of the *gli521* (P476R), m6, m27, m29, and m34 mutants were significantly reduced to 64–81% of that of the WT strain ($p = 6 \times 10^{-3}$, 4×10^{-4}, 9×10^{-5}, 8×10^{-9}, and 4×10^{-4}, respectively; $p < 0.01$, according to Student's *t*-test) (Fig. 2 *B*, *inset*). The *gli521* (P476R) mutant, which was characterized by enhanced binding, exhibited a smaller force than the WT strain, suggesting that the stability of binding is not the only determinant of stall force.

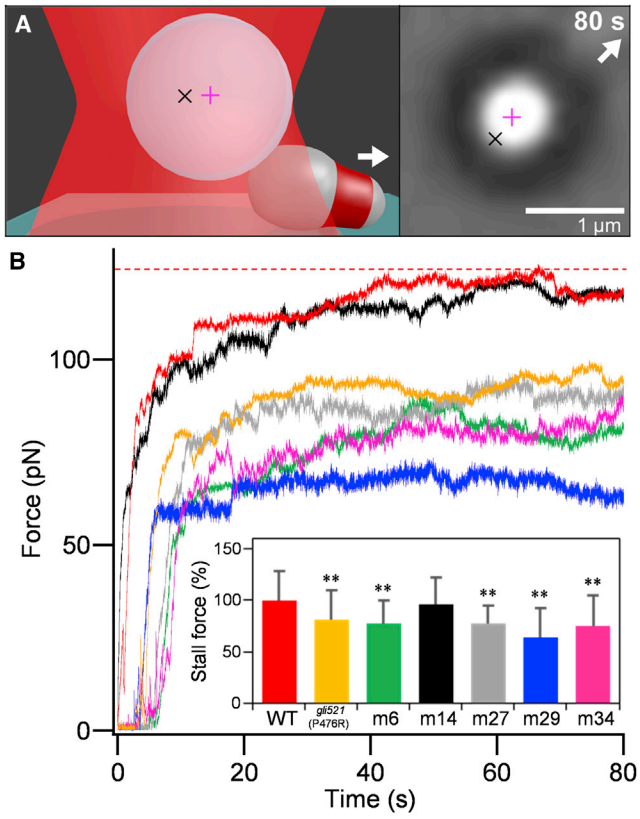

FIGURE 2 Stall force of the various strains. (*A*) On the left is an illustration of measurement using optical tweezers. The polystyrene bead (*circle*) (1.0 μm in diameter) bound to the cell is trapped by a focused laser beam (*red hourglass*) and glides in the direction of the white arrow. Black and pink crosses indicate the focal point of the laser and the bead center, respectively. On the right are optical micrographs of the trapped cell. The cell with the bead (large *black ring* with *white* center) was trapped at 0 s and stalled at 40 s. (*B*) Representative traces are shown. The line colors correspond to the bars in the inset. Shown in the inset are averages that were normalized to the WT value, and they are presented with standard deviations (SDs) ($n = 50$, 42, 26, 31, and 35). $^{**}p < 0.01$ (the difference from the WT was supported by Student's *t*-test). The red broken line indicates the stall force for the WT. To see this figure in color, go online.

Genome sequencing of various strains

To determine the proteins and mutations associated with the decreases in stall force, we sequenced the genomes of the strains using a MiSeq sequencer. The genome of the *gli521* (P476R) mutant has been sequenced for a 30,469-bp DNA region encoding four open reading frames: *gli123*, *gli349*, *gli521*, and *gli42*. However, the other regions remain unknown (21,35). The genome sequencing result for the *gli521* (P476R) mutant was consistent with the previous report of the mutation in *gli521* (21) and showed additional mutations in other regions (see Table S1). One of the additional mutations causes an amino acid substitution in MvspB, a surface protein (23,39–42). However, the reduced stall force should be caused by the mutation in Gli521 because MvspB accounts for only 1.2% of the mass of all the surface proteins, and the antibody against an abundant and closely related protein, MvspI, did not influence the gliding motility (23,42). The genomes of the m6, m14, m27, m29, and m34 strains have not been sequenced yet, and we identified various mutations in this study. We suggest that the decrease in the stall force in the m27 strain in this study was caused by the mutation in *gli521*. All the strains had the same single-amino-acid substitution (serine to isoleucine) as the 354th residue in MMOB1700, a homolog of ATP binding cassette transporter permease based on a Basic Local Alignment Search Tool search. This mutation may have been derived from a substitution that occurred on the clone used for the reported genome sequencing because it was derived from the same origin (American Type Culture Collection 43663) that was used in this study (39). Interestingly, MMOB1700 exhibited 5 other mutations in the 10 strains analyzed, suggesting a special mechanism that causes a high rate of mutation in this gene. Next, we sequenced the genomes of nonbinding strains m12, m13, and m23, which have mutations in *gli123*, *gli349*, and *gli349*, respectively (12,15,16,35). Genome sequencing

revealed that the identified mutations were consistent with a previous report (35), although additional mutations were identified in other regions.

Binding and gliding of various strains

To systematically clarify the relationship between the features and mutation in the genome, we examined the binding activities and the gliding speeds for the WT, *gli521* (P476R), m6, m14, m27, m29, and m34 mutants, which can glide. The cell suspensions were adjusted to the same optical density and inserted into a tunnel chamber. After 15 min, we videoed the cells to count the numbers on the glass for the bound-cell ratio and to determine their gliding speed, as previously reported (Fig. 3 *A*) (28,30,35). The binding activities and the gliding speeds were averaged for 20 independent images and 100 cells, respectively. The binding activity and gliding speed of the *gli521* (P476R) mutant were consistent with those reported in the previous study (35). Other strains have not been analyzed by the method used here. The characteristics of the binding activities allowed classification of the strains into three groups (Fig. 3 *B*, *left*): 1) m6 had 44% of the activity of the WT strain; 2) m14, m27, and m29 had 80, 92, and 73% of the activity, respectively; and 3) the *gli521* (P476R) and m34 mutants had 159 and 145% of the activity of the WT strain, respectively. We compared these data to the binding activities previously estimated from hemadsorption, the adsorption of erythrocytes onto the surface of colonies (12). The hemadsorption values of m6, m14, m27, m29, and m34 were 24, 93, 113, 96, and 122%, respectively; i.e., except for m27, they were consistent with the results of the analyses in this study. The gliding speed of the WT strain was 3.7 $\pm$ 0.2 μm/s, and the relative gliding speeds of the mutants ranged from 80 to 103% of the WT strain, showing that the gliding speeds differed less than the binding activities (Fig. 3 *B*, *right*). Of the strains enhanced for binding, the *gli521* (P476R) and m34 mutants had reduced stall forces, suggesting that stall force is not determined simply by binding activity.

Interestingly, we noticed that the proportions of the nongliding bound cells were much higher in the m6, m14, m27, and m29 strains than in the WT strain. The proportion of nongliding cells in the cells on glass was 6% for the WT strain, as previously reported (28), but those for the m6, m14, and m29 strains were higher (18, 19, and 16%, respectively) and that of the m27 strain was much higher (62%) (Fig. S1). This observation can be explained by assuming that gliding can be achieved by the concerted action of many molecules and interactions.

Effect of SOs on stall force

An *M. mobile* cell glides as a result of the integrated movement of its many legs. However, if the number of working legs is reduced, it is possible to detect the pulling force of a single unit. Previous studies have shown that the number of working legs can be reduced by adding free SOs (9,22,25,27,28,43). We therefore added various concentrations of free SL—an SO—to gliding *M. mobile* cells and measured the stall force at 200 and 500 frames per second with 0–0.25, 0.33, and 0.5 mM free SL. The cells reached a plateau after 30–40 s, and the time taken to reach the stall increased with the concentration of free SL. The stall force decreased from 113 to 19 pN after the addition of up to 0.50 mM free SL (Fig. 4, *A* and *B*). These results suggest that the stall force is the sum of the pulling force of many units.

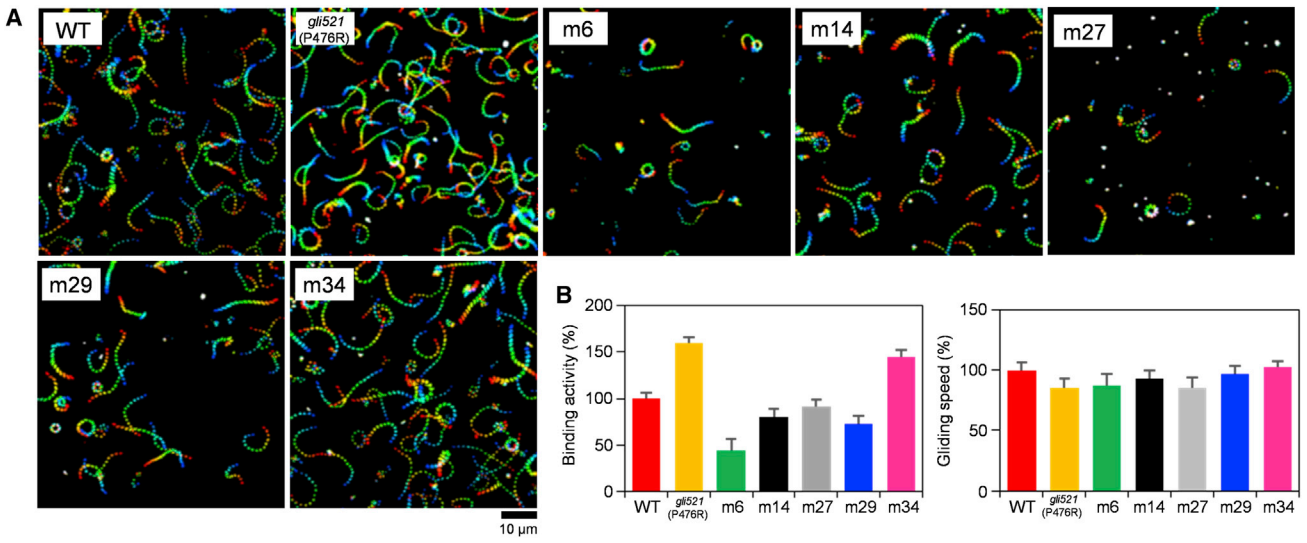

FIGURE 3 Binding and gliding properties of the various strains. (*A*) The cell trajectories are presented as a stack for 5 s, changing color from red to blue. (*B*) Averages of binding activity (*left*) and gliding speed (*right*) were normalized to the WT value and are presented with SDs. To see this figure in color, go online.

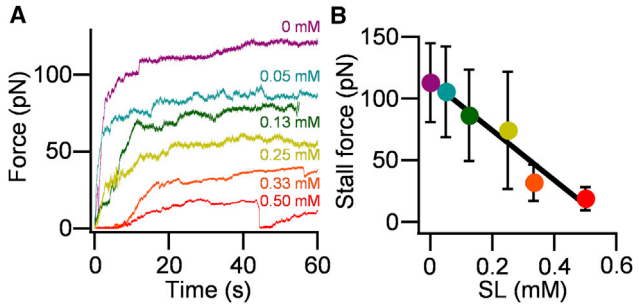

FIGURE 4 Effect of SL on stall force. (*A*) Representative traces at various concentrations of SL are shown by the numbers adjacent to the traces; these are colored the same way in (*B*). (*B*) Shown is the concentration dependency on SL. Averages were plotted with SDs ($n = 50$, 13, 23, 16, 16, and 11 for 0, 0.05, 0.13, 0.25, 0.33, and 0.50 mM, respectively). To see this figure in color, go online.

To detect the pulling force attributable to smaller numbers of units, we reduced the laser power of the optical tweezers to achieve a higher trace resolution. In this experiment, we applied 0.25 mM SL with a reduction of the trap stiffness of the optical tweezers from 0.5–0.7 to 0.1 pN/nm, whereby the trapped cells were able to escape from the trap center, and then measured the force under these conditions. The force increments with repeated small peaks were detected, and the peaks were measured using a peak-finding algorithm, as summarized in Fig. 5 *A*. The distribution of these increments was determined by fitting the sum of four Gaussian curves whose peaks were positioned at 1.1, 2.0, 3.2, and 4.4 pN (Fig. 5 *B*). The second to forth peaks were positioned at twice, three, and four times the value of the first peak, suggesting that these peaks reflect single, double, triple, and quadruple the minimal force increment (44). In the same way, the individual increments were analyzed for the *gli521* (P476R) mutant and were also determined by fitting the sum of four Gaussian curves whose peaks were positioned at 0.9, 1.8, 2.6, and 3.5 pN (Fig. 5 *B*).

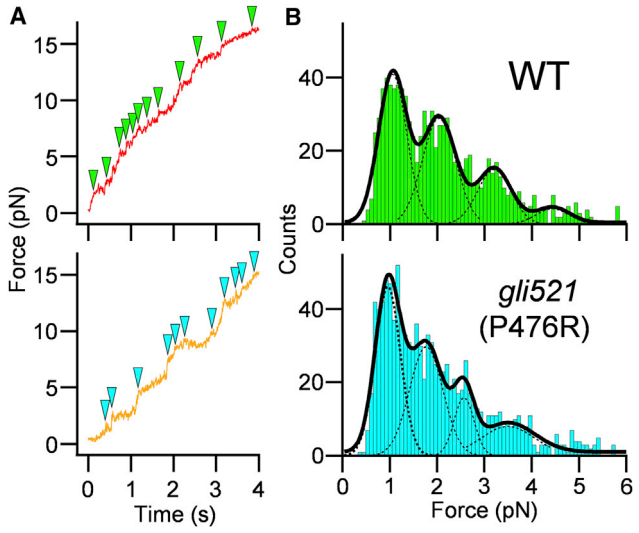

FIGURE 5 Detection of force increments under low load and 0.25 mM SL. (*A*) Representative traces of force transition in the WT and *gli521* (P476R) mutants are shown in the upper and lower panels, respectively. Green and cyan triangles in each panel indicate small peak positions taken by a peak-finding algorithm adapted to IGOR Pro 6.33J. (*B*) Distributions of peak values detected by the peak-finding algorithm were fitted to the sum of four Gaussian curves (*solid line*). The first, second, third, and fourth tops of the Gaussian curves (*dashed lines*) were 1.1, 2.0, 3.2, and 4.4 pN in the WT and 1.0, 1.8, 2.6, and 3.5 pN in the *gli521* (P476R) mutant, respectively ($n = 976$ and 1067). To see this figure in color, go online.

In these analyses, we traced cells by the displacements of beads because of their ease to trace. The distance between the cell and the attached bead did not change significantly in the trace (Fig. S2) under the trap conditions used for Figs. 5 and 6.

Stepwise force increments

Because the force increments were detected for limited leg numbers, it was possible to derive the force increments from the force generated by a single unit or a minimal force generation unit. Next, we added 0.50 mM SL to limit the number of working legs and reduced the trap stiffness to 0.06–0.07 pN/nm to detect the minimal force increments more precisely. Very small ratios of cells remained on the glass surface under these conditions, and we attached a bead to the cells using the optical tweezers. Displacements were detected in 51 of 63 cells. Eight cells glided by creeping displacements with occasional discontinuous increments, which were mostly stepwise (Fig. 6 *A*) and sometimes exhibited small peaks, as shown in Fig. 5. Three cells exhibited force increments with more than six continuous steps (Fig. 6 *B*; see also Movie S2). The average value of the force increments from 46 steps or peaks in 11 cell trajectories was 1.45 ± 0.44 pN (Fig. 6 *C*). These results suggest that the minimal force increment was 1–2 pN, which should be the minimal unit force for gliding.

DISCUSSION

Mutations influencing gliding

In this study, we sequenced the whole genomes of *M. mobile* mutants characterized by binding ability, gliding motility, and colony spreading (Figs. 2 and 3; see also Table S1) (12,21,35). Based on these results, we propose the proteins responsible for or related to these characteristics. The m6 strain, which exhibited reduced binding, a slower gliding speed, and a weaker stall force, has mutations in FtsH, MvspI, and SecY (40–42,45,46). The substituted amino acid in FtsH is not conserved in other mycoplasmas except for *Mycoplasma pulmonis*, a closely related species. MvspI is probably not involved in gliding, as described above (23). SecY is generally essential for protein secretion in bacteria (46). The substitution in SecY probably affects the secretion of gliding proteins, resulting in a reduction in the binding

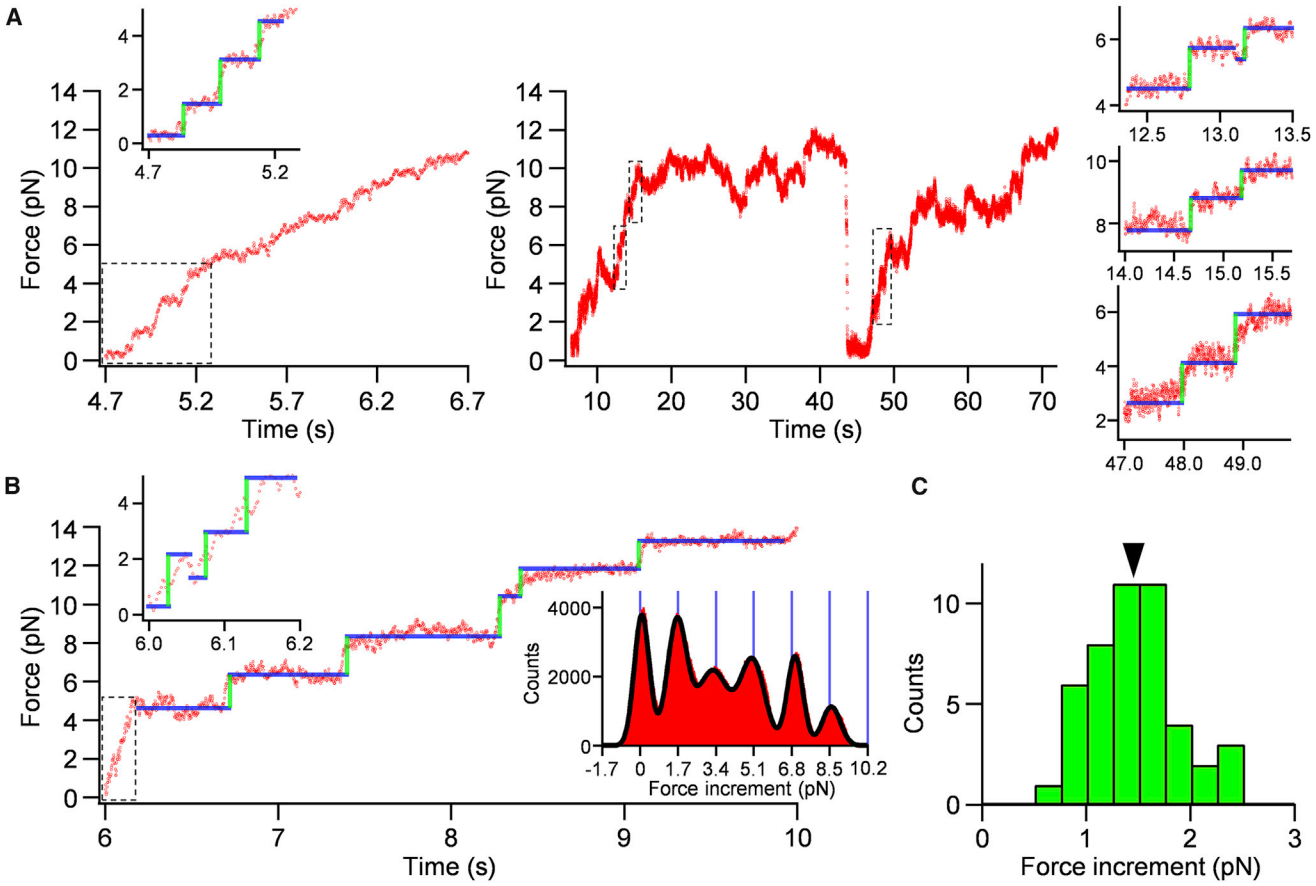

FIGURE 6 Detection of force increments under low load and 0.50 mM SL. (*A*) Two representative time courses of force generation are shown. The trajectories in the dashed rectangular areas are magnified as insets and marked as green and blue lines for increments and dwell times, respectively. (*B*) A representative time course of continuous stepwise trajectory is shown. The histogram of pairwise distance function analysis for indicated steps is shown in the right inset. (*C*) The histogram of force increments for 46 steps or peaks is shown. The averaged value is indicated by a black triangle. To see this figure in color, go online.

activity of cells, because the amino acid substituted in the mutant is conserved in many mycoplasmas, including *Mycoplasma hominis*, *Mycoplasma bovis*, and *M. pulmonis*. The m14 strain was characterized by slightly reduced binding and gliding, and its glucokinase, which phosphorylates glucose to glucose-6-phosphate at the first step of glycolysis, has an amino acid substitution (47). The less effective glycolysis may cause the reduction of binding and gliding. Interestingly, the m14 colony was less well dispersed than the WT colony, suggesting that this glucokinase is related to chemotaxis because colony shape is also largely influenced by chemotaxis in many bacteria (12). Actually, a novel chemotaxis mechanism unrelated to the two-component system has been suggested for the class *Mollicutes* (48–50). The m27 strain, which was characterized by a small proportion of gliding cells, has a substitution at the 1461st amino acid out of a total of 4727 amino acids in the coded Gli521 protein, suggesting that the structure around this position is indispensable for gliding. The m34 strain was characterized by enhanced binding and has a substitution in the conserved amino acid of the β-subunit of F-type ATPase (51). The F-type ATPase is thought to function primarily in the maintenance of membrane potential in *Mycoplasma* species because respiration systems do not exist in mycoplasmas (51). Gli349, the leg protein, is foldable and negatively charged, and needs to raise when it catches SOs (15,18,26,52). The genome sequence of m34 suggests that the membrane potential may influence the binding activity of Gli349 through the folding states of the molecule.

Cell behavior in the stall

Each cell was stalled using optical tweezers focused on the bead that was bound to the back end of the cell. What events can be expected in the stall? The stall force decreased with the addition of free SL (Fig. 4). This observation suggests that the legs repeatedly catch, pull, and release SOs even in the stalled state (Fig. 7), as suggested for free-load gliding (Fig. 1 *A*), because the force under free SOs should increase and reach the value of stall force in the absence of SOs if the legs do not detach in stall. In our gliding model, it was suggested that the legs detach as a result of the tension caused

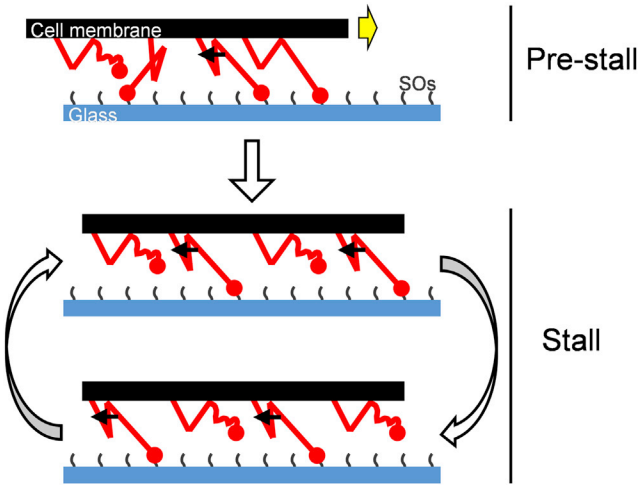

FIGURE 7 Leg behavior during stall. During pre-stall, the legs colored red repeatedly catch, pull, drag, and release the SOs on the glass surface, thereby enabling cell propulsion. During stall, the force-transmitting legs are in equilibrium between attached and released states. The yellow and black arrows indicate the gliding direction and the pulling force transmitted through the leg strokes, respectively. To see this figure in color, go online.

by continuous cell displacement in gliding (Fig. 1 *A*) (14,29,43). The putative detachment in the stall may suggest that directed detachment occurs with much shorter displacement than expected from a 95-nm-long leg structure because the detachment also occurs in the stall. This assumption can explain the observation that the *gli521* (P476R) and m34 mutants exhibited a smaller stall force than the WT strain although they had a higher ratio of cells bound to the glass (Figs. 2 and 3). The higher ratio of bound cells was probably due to the reduction in the pulling force applicable to detach the poststroke legs, causing their prolonged stay on SOs. In the case of the m6 mutant, the legs may release SOs by a smaller force.

Unit number of gliding machinery

The minimal force increment did not change significantly with the distance from the laser. Because the force increments occurred additionally to the previous ones, the gliding unit should have generated the same force constantly over a rather long distance ranging from 0 to 200 nm (Fig. 6). Alternatively, the increment may include detachment of a unit.

In this study, the stall force and the minimal force increments of a cell were ~113 and 1.5 pN, respectively (Figs. 2 *B* and 6 *C*). Previously, the number of legs in *M. mobile* was estimated to be 450 (16). The number of working units was calculated from the stall force and the minimal force increments of a cell; 113 over 1.5 pN is calculated to be ~75-fold, suggesting that 75 minimal units can work simultaneously. Assuming that the minimal unit of force corresponds to a single molecule of Gli349, one-sixth of the Gli349 molecules are suggested to simultaneously participate in force generation in the stalled state (Fig. 1 *B*). The friction occurring at the interface between an *M. mobile* cell and water flow in the interlamellar space of a carp gill is calculated to be 34 pN for the maximum, based on Stokes' law (11,53). This number is threefold smaller than the stall force of a cell, suggesting that a cell can glide against water flow using the force transmitted through many legs.

M. mobile gliding is characterized by large steps and a small force

We compared the step size and the force of *M. mobile* gliding with those of conventional motor proteins such as myosin, dynein, and kinesin, which perform stepwise movements along the rail proteins driven by the energy derived from ATP. The step sizes and the forces of myosin-II, cytoplasmic dynein, kinesin, and myosin-V have been reported as 5.3, 8, 8, and 36 nm and 3–5, 7–8, 8, and 2–3 pN, respectively (54–59). The long step and small force of myosin-V are caused by the lever effect of 26-nm arms (60). The step size of *M. mobile* is 70 nm, much larger than that of conventional motor proteins (22). The minimal unit force calculated here (1–2 pN) suggests the gear effect in the gliding machinery. Gli521, which is the force transmitter, forms a triskelion with 100-nm arms (24), and Gli349, which is the leg, is shaped like an eighth note in musical notation, with a 43-nm flexible string (26,61). The small movements generated in the internal motor may be amplified to achieve a 70-nm step by the lever effects through these large proteins.

Energy conversion efficiency of *M. mobile* gliding

The direct energy source for *M. mobile* gliding is ATP; based on experiments that permeabilize cells, a "gliding ghost" can be reactivated by ATP (21). A gliding ghost exhibits stepwise movement, with a dwell time that is dependent on the ATP concentration used, suggesting that the step is coupled to ATP hydrolysis (22). Based on a minimal unit force of 1–2 pN and a spring constant of 0.06–0.07 pN/nm, the work done per step (W_{step} in the experiments under the condition in Fig. 6) is calculated to be 8–33 pN nm from the equation $W_{step} = 0.5 \times \text{spring constant} \times \text{displacement}^2$. Assuming that one ATP molecule is consumed per step, the energy conversion efficiency of *M. mobile* gliding can be calculated to be ~10–40% because generally ~80 pN nm free energy is available from the hydrolysis of one ATP molecule.

F-type ATPase attains 100% energy conversion efficiency (62). It has been suggested that the gliding machinery of *M. mobile* is driven by the α- and β-subunit paralogs of F-type ATPase (18). The force transmission from this motor to the solid surfaces through several large components, including Gli521 and Gli349, may be related to the putative energy loss.

SUPPORTING MATERIAL

Two figures, one table, and two movies are available at http://www.biophysj.org/biophysj/supplemental/S0006-3495(18)30188-7.

AUTHOR CONTRIBUTIONS

M. Mizutani and M. Miyata designed the research. M. Mizutani and I.T. analyzed the genomes. M. Mizutani did all other experiments. M. Mizutani, Y.K., T.N., and M. Miyata contributed to interpretation of force measurement results. M. Mizutani and M. Miyata drafted the main manuscript, and all authors reviewed it.

ACKNOWLEDGMENTS

This work was supported by a Grant-in-Aid for Scientific Research in the innovative area "Harmonized Supramolecular Motility Machinery and Its Diversity" (Ministry of Education, Culture, Sports, Science and Technology KAKENHI; grant number 24117002) and by Grants-in-Aid for Scientific Research (B) and (A) (Ministry of Education, Culture, Sports, Science and Technology KAKENHI; grant numbers 24390107 and 17H01544) to M. Miyata.

REFERENCES

1. Razin, S., D. Yogev, and Y. Naot. 1998. Molecular biology and pathogenicity of mycoplasmas. *Microbiol. Mol. Biol. Rev.* 62:1094–1156.
2. Razin, S., and L. Hayflick. 2010. Highlights of mycoplasma research–an historical perspective. *Biologicals.* 38:183–190.
3. Miyata, M. 2008. Centipede and inchworm models to explain *Mycoplasma* gliding. *Trends Microbiol.* 16:6–12.
4. Miyata, M. 2010. Unique centipede mechanism of *Mycoplasma* gliding. *Annu. Rev. Microbiol.* 64:519–537.
5. Miyata, M., and T. Hamaguchi. 2016. Prospects for the gliding mechanism of *Mycoplasma mobile*. *Curr. Opin. Microbiol.* 29:15–21.
6. Nakane, D., T. Kenri, …, M. Miyata. 2015. Systematic structural analyses of attachment organelle in *Mycoplasma pneumoniae*. *PLoS Pathog.* 11:e1005299.
7. Miyata, M., and T. Hamaguchi. 2016. Integrated information and prospects for gliding mechanism of the pathogenic bacterium *Mycoplasma pneumoniae*. *Front. Microbiol.* 7:960.
8. Kawamoto, A., L. Matsuo, …, M. Miyata. 2016. Periodicity in attachment organelle revealed by electron cryotomography suggests conformational changes in gliding mechanism of *Mycoplasma pneumoniae*. *MBio.* 7:e00243–16.
9. Morio, H., T. Kasai, and M. Miyata. 2015. Gliding direction of *Mycoplasma mobile*. *J. Bacteriol.* 198:283–290.
10. Lee, W., Y. Kinosita, …, D. Kim. 2015. Three-dimensional superlocalization imaging of gliding *Mycoplasma mobile* by extraordinary light transmission through arrayed nanoholes. *ACS Nano.* 9:10896–10908.
11. Miyata, M., W. S. Ryu, and H. C. Berg. 2002. Force and velocity of *Mycoplasma mobile* gliding. *J. Bacteriol.* 184:1827–1831.
12. Miyata, M., H. Yamamoto, …, R. Rosengarten. 2000. Gliding mutants of *Mycoplasma mobile*: relationships between motility and cell morphology, cell adhesion and microcolony formation. *Microbiology.* 146:1311–1320.
13. Rosengarten, R., and H. Kirchhoff. 1987. Gliding motility of *Mycoplasma* sp. nov. strain 163K. *J. Bacteriol.* 169:1891–1898.
14. Chen, J., J. Neu, …, G. Oster. 2009. Motor-substrate interactions in mycoplasma motility explains non-Arrhenius temperature dependence. *Biophys. J.* 97:2930–2938.
15. Uenoyama, A., A. Kusumoto, and M. Miyata. 2004. Identification of a 349-kilodalton protein (Gli349) responsible for cytadherence and glass binding during gliding of *Mycoplasma mobile*. *J. Bacteriol.* 186:1537–1545.
16. Uenoyama, A., and M. Miyata. 2005. Identification of a 123-kilodalton protein (Gli123) involved in machinery for gliding motility of *Mycoplasma mobile*. *J. Bacteriol.* 187:5578–5584.
17. Seto, S., A. Uenoyama, and M. Miyata. 2005. Identification of a 521-kilodalton protein (Gli521) involved in force generation or force transmission for *Mycoplasma mobile* gliding. *J. Bacteriol.* 187:3502–3510.
18. Nakane, D., and M. Miyata. 2007. Cytoskeletal "jellyfish" structure of *Mycoplasma mobile*. *Proc. Natl. Acad. Sci. USA.* 104:19518–19523.
19. Tulum, I., M. Yabe, …, M. Miyata. 2014. Localization of P42 and F_1-ATPase α-subunit homolog of the gliding machinery in *Mycoplasma mobile* revealed by newly developed gene manipulation and fluorescent protein tagging. *J. Bacteriol.* 196:1815–1824.
20. Jaffe, J. D., M. Miyata, and H. C. Berg. 2004. Energetics of gliding motility in *Mycoplasma mobile*. *J. Bacteriol.* 186:4254–4261.
21. Uenoyama, A., and M. Miyata. 2005. Gliding ghosts of *Mycoplasma mobile*. *Proc. Natl. Acad. Sci. USA.* 102:12754–12758.
22. Kinosita, Y., D. Nakane, …, T. Nishizaka. 2014. Unitary step of gliding machinery in *Mycoplasma mobile*. *Proc. Natl. Acad. Sci. USA.* 111:8601–8606.
23. Kusumoto, A., S. Seto, …, M. Miyata. 2004. Cell surface differentiation of *Mycoplasma mobile* visualized by surface protein localization. *Microbiology.* 150:4001–4008.
24. Nonaka, T., J. Adan-Kubo, and M. Miyata. 2010. Triskelion structure of the Gli521 protein, involved in the gliding mechanism of *Mycoplasma mobile*. *J. Bacteriol.* 192:636–642.
25. Nagai, R., and M. Miyata. 2006. Gliding motility of *Mycoplasma mobile* can occur by repeated binding to *N*-acetylneuraminyllactose (sialyllactose) fixed on solid surfaces. *J. Bacteriol.* 188:6469–6475.
26. Adan-Kubo, J., A. Uenoyama, …, M. Miyata. 2006. Morphology of isolated Gli349, a leg protein responsible for *Mycoplasma mobile* gliding via glass binding, revealed by rotary shadowing electron microscopy. *J. Bacteriol.* 188:2821–2828.
27. Kasai, T., D. Nakane, …, M. Miyata. 2013. Role of binding in *Mycoplasma mobile* and *Mycoplasma pneumoniae* gliding analyzed through inhibition by synthesized sialylated compounds. *J. Bacteriol.* 195:429–435.
28. Kasai, T., T. Hamaguchi, and M. Miyata. 2015. Gliding motility of *Mycoplasma mobile* on uniform oligosaccharides. *J. Bacteriol.* 197:2952–2957.
29. Tanaka, A., D. Nakane, …, M. Miyata. 2016. Directed binding of gliding bacterium, *Mycoplasma mobile*, shown by detachment force and bond lifetime. *MBio.* 7:e00455-16.
30. Nakane, D., and M. Miyata. 2012. *Mycoplasma mobile* cells elongated by detergent and their pivoting movements in gliding. *J. Bacteriol.* 194:122–130.
31. Ashkin, A., J. M. Dziedzic, …, S. Chu. 1986. Observation of a single-beam gradient force optical trap for dielectric particles. *Opt. Lett.* 11:288.
32. Nishizaka, T., H. Miyata, …, K. Kinosita, Jr. 1995. Unbinding force of a single motor molecule of muscle measured using optical tweezers. *Nature.* 377:251–254.
33. Mizutani, M., and M. Miyata. 2017. Force measurement on *Mycoplasma mobile* gliding using optical tweezers. *Bio Protoc.* 7:e2127.
34. Aluotto, B. B., R. G. Wittler, …, J. E. Faber. 1970. Standardized bacteriologic techniques for the characterization of *Mycoplasma* species. *Int. J. Syst. Bacteriol.* 20:35–58.
35. Uenoyama, A., S. Seto, …, M. Miyata. 2009. Regions on Gli349 and Gli521 protein molecules directly involved in movements of *Mycoplasma mobile* gliding machinery, suggested by use of inhibitory antibodies and mutants. *J. Bacteriol.* 191:1982–1985.

36. Hiratsuka, Y., M. Miyata, and T. Q. Uyeda. 2005. Living microtransporter by uni-directional gliding of *Mycoplasma* along microtracks. *Biochem. Biophys. Res. Commun.* 331:318–324.

37. Hiratsuka, Y., M. Miyata, …, T. Q. Uyeda. 2006. A microrotary motor powered by bacteria. *Proc. Natl. Acad. Sci. USA.* 103:13618–13623.

38. Kinosita, Y., N. Uchida, …, T. Nishizaka. 2016. Direct observation of rotation and steps of the archaellum in the swimming halophilic archaeon *Halobacterium salinarum*. *Nat. Microbiol.* 1:16148.

39. Jaffe, J. D., N. Stange-Thomann, …, G. M. Church. 2004. The complete genome and proteome of *Mycoplasma mobile*. *Genome Res.* 14:1447–1461.

40. Adan-Kubo, J., S. H. Yoshii, …, M. Miyata. 2012. Molecular structure of isolated MvspI, a variable surface protein of the fish pathogen *Mycoplasma mobile*. *J. Bacteriol.* 194:3050–3057.

41. Wu, H. N., C. Kawaguchi, …, M. Miyata. 2012. "Mycoplasmal antigen modulation," a novel surface variation suggested for a lipoprotein specifically localized on *Mycoplasma mobile*. *Curr. Microbiol.* 64:433–440.

42. Wu, H. N., and M. Miyata. 2012. Whole surface image of *Mycoplasma mobile*, suggested by protein identification and immunofluorescence microscopy. *J. Bacteriol.* 194:5848–5855.

43. Kasai, T., and M. Miyata. 2013. Analyzing inhibitory effects of reagents on *Mycoplasma* gliding and adhesion. *Bio Protoc.* 3:e829.

44. Leidel, C., R. A. Longoria, …, G. T. Shubeita. 2012. Measuring molecular motor forces in vivo: implications for tug-of-war models of bidirectional transport. *Biophys. J.* 103:492–500.

45. Ito, K., and Y. Akiyama. 2005. Cellular functions, mechanism of action, and regulation of FtsH protease. *Annu. Rev. Microbiol.* 59:211–231.

46. Mori, H., and K. Ito. 2006. Different modes of SecY-SecA interactions revealed by site-directed in vivo photo-cross-linking. *Proc. Natl. Acad. Sci. USA.* 103:16159–16164.

47. Gaurivaud, P., E. Baranowski, …, F. Tardy. 2016. *Mycoplasma agalactiae* secretion of beta-(1→6)-glucan, a rare polysaccharide in prokaryotes, is governed by high-frequency phase variation. *Appl. Environ. Microbiol.* 82:3370–3383.

48. Daniels, M. J., J. M. Longland, and J. Gilbart. 1980. Aspects of motility and chemotaxis in spiroplasmas. *J. Gen. Microbiol.* 118:429–436.

49. Daniels, M. J., and J. M. Longland. 1984. Chemotactic behavior of spiroplasmas. *Curr. Microbiol.* 10:191–193.

50. Liu, P., H. Zheng, …, M. Miyata. 2017. Chemotaxis without conventional two-component system, based on cell polarity and aerobic conditions in helicity-switching swimming of *Spiroplasma eriocheiris*. *Front. Microbiol.* 8:58.

51. Béven, L., C. Charenton, …, P. Sirand-Pugnet. 2012. Specific evolution of F_1-like ATPases in mycoplasmas. *PLoS One.* 7:e38793.

52. Miyata, M., and J. D. Petersen. 2004. Spike structure at the interface between gliding *Mycoplasma mobile* cells and glass surfaces visualized by rapid-freeze-and-fracture electron microscopy. *J. Bacteriol.* 186:4382–4386.

53. Lauder, G. V. 1984. Pressure and water flow patterns in the respiratory tract of the bass (*Micropterus salmoides*). *J. Exp. Biol.* 113:151–164.

54. Schnitzer, M. J., and S. M. Block. 1997. Kinesin hydrolyses one ATP per 8-nm step. *Nature.* 388:386–390.

55. Kojima, H., E. Muto, …, T. Yanagida. 1997. Mechanics of single kinesin molecules measured by optical trapping nanometry. *Biophys. J.* 73:2012–2022.

56. Takagi, Y., E. E. Homsher, …, H. Shuman. 2006. Force generation in single conventional actomyosin complexes under high dynamic load. *Biophys. J.* 90:1295–1307.

57. Fujita, K., M. Iwaki, …, T. Yanagida. 2012. Switching of myosin-V motion between the lever-arm swing and Brownian search-and-catch. *Nat. Commun.* 3:956.

58. Park, P. J., and K. J. Lee. 2013. A modified active Brownian dynamics model using asymmetric energy conversion and its application to the molecular motor system. *J. Biol. Phys.* 39:439–452.

59. Gennerich, A., A. P. Carter, …, R. D. Vale. 2007. Force-induced bidirectional stepping of cytoplasmic dynein. *Cell.* 131:952–965.

60. Vilfan, A. 2005. Elastic lever-arm model for myosin V. *Biophys. J.* 88:3792–3805.

61. Metsugi, S., A. Uenoyama, …, N. Go. 2005. Sequence analysis of the gliding protein Gli349 in *Mycoplasma mobile*. *Biophysics (Nagoya-shi).* 1:33–43.

62. Kinosita, K., Jr., R. Yasuda, …, K. Adachi. 2000. A rotary molecular motor that can work at near 100% efficiency. *Philos. Trans. R. Soc. Lond. B Biol. Sci.* 355:473–489.